Modeling and Simulation of Bacterial Outer Membranes with Lipopolysaccharides and Enterobacterial Common Antigen

Ya Gao^{1,2}, Jumin Lee², Göran Widmalm^{3*}, and Wonpil Im^{2,4*}

¹School of Mathematics, Physics and Statistics, Shanghai University of Engineering Science, Shanghai 201620, China

²Department of Biological Sciences, Department of Chemistry, and Department of Bioengineering, Lehigh University, Bethlehem, PA 18015, USA

³Department of Organic Chemistry, Arrhenius Laboratory, Stockholm University, SE-10691 Stockholm, Sweden

⁴School of Computational Sciences, Korea Institute for Advanced Study, Seoul 02455, Republic of Korea

*Corresponding author e-mail: Goran.Widmalm@su.se and wonpil@lehigh.edu

Abstract

Enterobacterial common antigen (ECA) is a surface glycolipid shared by all members of the Enterobacteriaceae family. In addition to lipopolysaccharides (LPS), ECA is an important component in the outer membrane (OM) of Gram-negative bacteria, making the OM an effective, selective barrier against the permeation of toxic molecules. Previous modeling and simulation studies represented OMs exclusively with LPS in the outer leaflet. In this work, various ECA molecules were first modeled and incorporated into symmetric bilayers with LPS in different ratios, and all-atom molecular dynamics simulations were conducted to investigate the properties of the mixed bilayers mimicking OM outer leaflets. Dynamic and flexible conformational ensembles are sampled for each ECA/LPS system. Incorporation of ECA_{LPS} (an LPS core-linked form) and ECA_{PG} (a phosphatidylglycerol-linked form) affects lipid packing and ECA/LPS distributions on the bilayer surface. Hydrophobic thickness and chain order parameter analyses indicate that incorporation of ECA_{PG} makes the acyl chains of LPS more flexible and disordered and thus increases the area per lipid of LPS. The calculated area per lipid of each ECA/LPS provides a good estimate for building more realistic OMs with different ratios of ECA/LPS, which will be useful in order to characterize their interactions with outer membrane proteins in more realistic OMs.

Introduction

Different from Gram-positive bacteria, the cell envelope surrounding the cytoplasm of Gram-negative bacteria is composed of the inner membrane, the periplasm, and the outer membrane (OM). The OM is a unique and asymmetric lipid bilayer that has phospholipids in the inner leaflet and mostly lipopolysaccharides (LPS) in the outer leaflet. LPS is a complex amphiphilic molecule consisting of the lipid A, core oligosaccharide, and O-antigen polysaccharide regions. In addition to LPS, there are glycolipids such as enterobacterial common antigen (ECA) and capsular polysaccharide (CPS) that are also important components in the OM outer leaflet, but their occurrence is frequently overlooked. These unique cell surface glycoconjugates make the OM an effective, selective barrier against the permeation of toxic molecules, playing a critical role in the biological functions of Gramnegative bacterial OMs. Modeling and simulation studies on the properties of various OMs or outer membrane proteins embedded in OMs have been reported recently by several research groups. As the outer leaflets of OMs are represented exclusively by LPS in these studies, incorporation of ECA and CPS is required for modeling and simulation of more realistic OMs.

ECA is a cell surface glycolipid expressed by Gram-negative bacteria belonging to the *Enterobacteriaceae* family, including emerging drug-resistant pathogens such as *Escherichia coli* (*E. coli*), *Klebsiella pneumoniae*, and *Proteus* spp. ¹⁷⁻¹⁸ As shown in **Figure 1**, the carbohydrate portion of ECA contains the amino sugars such as *N*-acetyl-D-glucosamine (GlcpNAc), *N*-acetyl-D-mannosaminuronic acid (ManpNAcA), and 4-acetamido-4,6-dideoxy-D-galactose (Fucp4NAc). These three amino sugars form a linear trisaccharide repeating unit, \rightarrow 3)- α -D-Fucp4NAc-(1 \rightarrow 4)- β -D-ManpNAcA-(1 \rightarrow 4)- α -D-GlcpNAc-(1 \rightarrow . ¹⁹⁻²⁰ ECA occurs in three forms, (i) a cyclic form (ECA_{CYC})²¹⁻²² localized to the periplasm, (ii) a phosphatidylglycerol (PG)-linked form (ECA_{PG}) located on the cell surface, ²³⁻²⁵ and (iii) an endotoxin/LPS-associated form (ECA_{LPS}) that is the only immunogenic form of ECA and capable of eliciting cross-reactive anti-ECA antibodies. ^{17, 21, 26} The biological significance of ECA is not fully understood. Thus, modeling and characterizing the OM with LPS and ECA at the molecular level is critical to better understand its biological functions and conformational properties.

In this work, both ECA_{PG} and ECA_{LPS} are first modeled and incorporated into various symmetric bilayers with LPS in different ratios, since the exact amount of ECAs in *Enterobacteriaceae* is unknown experimentally; ECA_{CYC} is not included as it exists in solution. Note that symmetric bilayer systems with the mixture of LPS and ECA were constructed and simulated to better characterize various bilayer properties such as hydrophobic thickness, chain order parameters, area per lipid, and the influence of ECA glycoconjugates on the LPS-only bilayer structure. This work forms the basis for future studies aimed at characterization of interactions between LPS, ECA, CPS, and outer membrane proteins in more realistic OMs.

Methods

The sequence of each LPS, ECALPS, and ECAPG used in this study is shown in Figure 1. E. coli lipid A and R1 core were used to model E. coli LPS and ECALPS. For ECAPG, acyl chains with 16:0 in C1 and 16:0 (dipalmitoyl phosphatidylglycerol: DPPG), 18:0 *cis*-11 (palmitoylstearoyl phosphatidylglycerol: PSPG), or 18:1 (palmitoylvacenoyl phosphatidylglycerol: PVPG) in C2 were used. Structures of E. coli lipid A, DPPG, PSPG, and PVPG are shown in Figure S1. A branched and negatively charged E. coli O159 O-antigen polysaccharide (O159 PS)²⁷ was used in the modeling of LPS, which is complementary to our previous studies that used linear neutral O176²⁸, branched neutral O6⁵, or linear negatively charged O917 O-antigen types. Five O159 PS and ten ECA PS repeating units (RUs) were used for O159 LPS and ECA_{LPS}/ECA_{PG}, respectively. To investigate the properties of ECAcontaining bilayers as well as the conformational properties of each ECA and LPS, symmetric O159 LPS bilayer systems mixed with 0%, 5%, 25%, and 50% of each ECA type were modeled and simulated. Table S1 summarizes detailed system information including the number of lipids in each leaflet. The pure O159 LPS system was generated using Membrane *Builder*²⁹⁻³³ in CHARMM-GUI (http://www.charmm-gui.org),³⁴ while mixed systems (containing ECA_{LPS} and ECA_{PG}) were built following the protocols of *Membrane Builder* using the premodeled structures of ECA_{LPS} and ECA_{PG}. Ca²⁺ ions were added to the LPS lipid A and core sugar residues to neutralize each system and 150 mM KCI was also added to the bulk region to mimic the bulk ion solution.

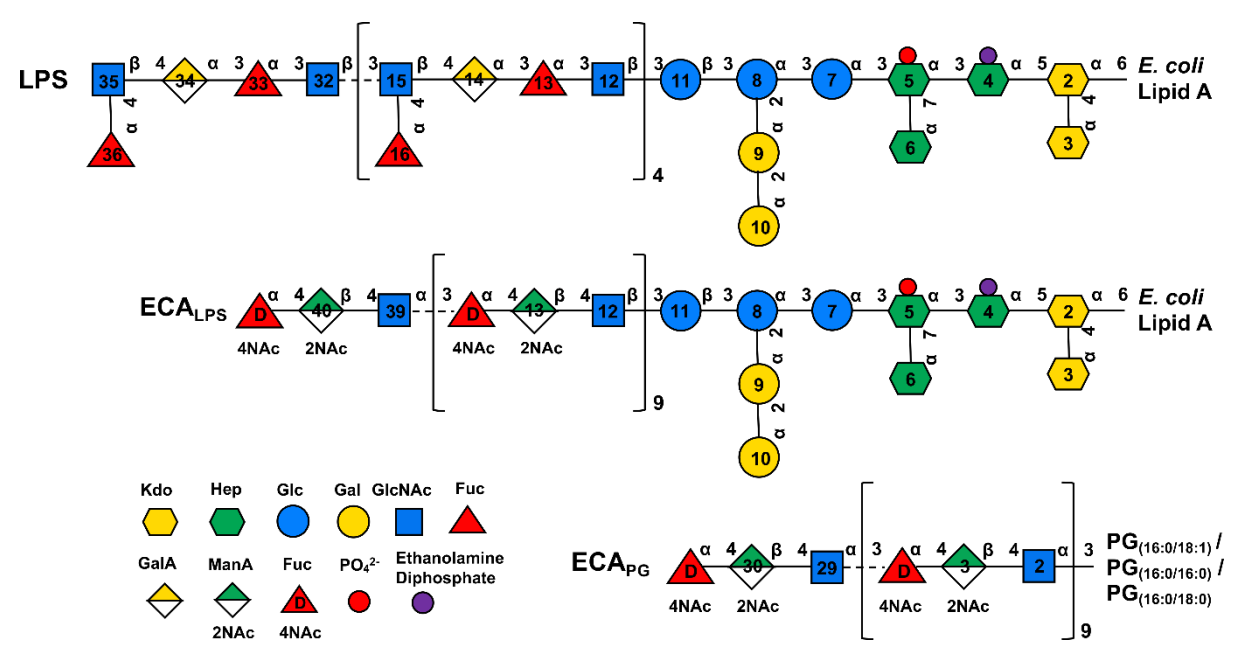


Figure 1. Schematic structures of *E. coli* O159 LPS having an R1 core, ECA_{LPS}, and ECA_{PG}. Chemical structures of lipid A, PVPG, DPPG, and PSPG are depicted in **Figure S1**.

The CHARMM36 force field for LPS, 35-36 lipids, 37 and carbohydrates 38-41 was used to describe the system energetics. For each system, equilibrations were first conducted by following the Membrane Builder equilibration protocol. Briefly, NVT (constant particle number, volume, and temperature) dynamics was first used and subsequently followed by NPT (constant particle number, pressure, and temperature) simulations. During the equilibration, gradually decreasing restraints were applied in six steps to the lipids and water molecules to assure the gradual equilibration of the assembled system. After equilibration, 1-µs production NPT simulation with 2-fs time-step was conducted for each system. All bonds to hydrogen atoms were fixed using the SHAKE algorithm. 42 The van der Waals interactions were smoothly switched off at 10-12 Å by a force-switching function⁴³ and the long-range electrostatic interactions were calculated using the particle-mesh Ewald method. 44 Langevin dynamics was used for the temperature coupling with a collision frequency of 1 ps⁻¹. A semi-isotropic Monte Carlo barostat method with a pressure coupling frequency of 100 steps was used to maintain the pressure. 45-46 The temperature was maintained at 303.15 K and the pressure was set to 1.0 bar. Three independent replicas with different random seed numbers were generated for each system to improve sampling and to check the simulation convergence. All simulations were conducted utilizing OpenMM.47

Results and Discussion

Conformational Variations of LPS and ECA

For each system, the variation of X or Y dimension length as a function of simulation time is shown in **Figure S2**; the membrane area is given by $X \times Y$. For most systems, three replicas show convergence within 500-ns simulations. There are also some slight deviations

among three replicas as these LPS-containing systems are well known for slow relaxation. Despite these minor sampling issues, the current simulations overall show good convergence (see below) for sufficient statistical analyses. Unless explicitly specified, the analysis was done using the last 500-ns trajectory.

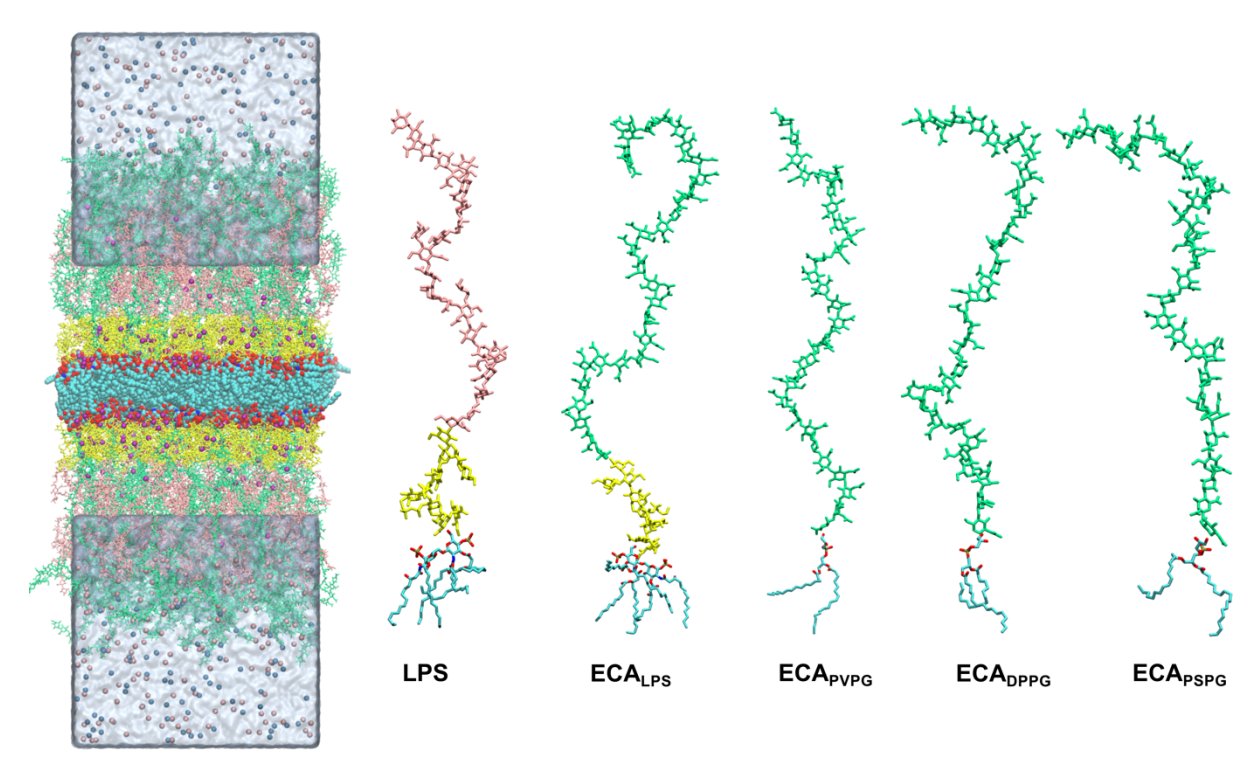


Figure 2. Molecular graphics snapshots of system ⁵⁰LPS²⁵ECA_{LPS}²⁵ECA_{PG} and each component. Lipid A, PVPG, DPPG, and PSPG in each LPS and ECA are colored by atom: cyan for carbon, red for oxygen, blue for nitrogen, and tan for phosphorus. The R1 core is colored yellow, five O159 polysaccharide (O159 PS) repeating units (RUs) are colored pink, and ten ECA PS RUs are colored green. Calcium, potassium, and chloride ions are shown as magenta, pink, and blue spheres. Water molecules are shown in transparent surface.

Pairwise root mean square deviation (RMSD) analysis for lipid and sugar portions of each LPS and ECA in each system was conducted to explore the conformation variations. As shown in **Figure S3**, dynamic and flexible conformations were sampled for lipid tails with RMSD peak located around 8 Å (lipid A) and 5 Å (phosphatidylglycerol lipids) in each system. Lipid tails of LPS and ECA_{PG} show more flexible conformations as there are more ECA_{PG} in the system, i.e., system ⁵⁰LPS⁵⁰ECA_{PG} (the superscripts for the population of each LPS and ECA) show the highest flexibility of lipid tails. This flexibility difference is related to other bilayer properties that are elaborated below. Due to their sizes, sugars in each LPS and ECA exhibit more flexible conformations compared to lipid tails, as shown by their broader RMSD distributions in **Figure S4**. **Figure 2** shows one representative snapshot of system ⁵⁰LPS²⁵ECA_{LPS}²⁵ECA_{PG}, in which LPS and ECA are flexible and dynamic but packed tightly forming the bilayer in simulations.

Figure 3 shows the density distribution of each component along the membrane normal (i.e., the Z-axis) in a representative $^{50}\text{LPS}^{25}\text{ECA}_{LPS}^{25}\text{ECA}_{PG}$ system. The number of LPS in the system is twice more than that of ECA_{LPS} or ECA_{PG}, so its density is higher than other two glycolipids as expected. In addition, the number of sugars (10 RUs x 3 sugars / RU) of ECA_{LPS} and ECA_{PG} are both larger than that of the O159 PS (5 RUs x 5 sugars / RU), so the RUs of ECA_{LPS} and ECA_{PG} have broader distributions along the Z axis. For the distribution of Ca²⁺ ions (**Figure S5**), it is dominantly occupied in the lipid headgroup and core regions,

maintaining the integrity of the membrane system, but some Ca^{2+} moved slightly toward the O-antigen region indicated by the small peak at Z = 50 Å.

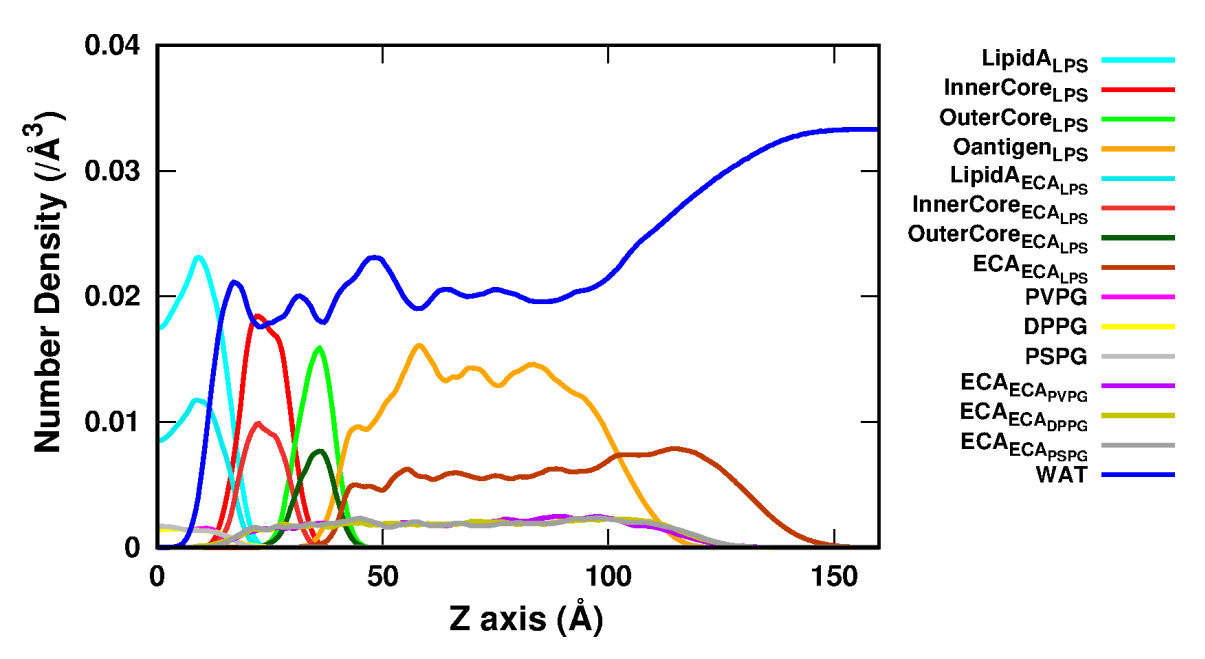


Figure 3. Density profiles along the Z-axis for different components of each LPS, ECA, and water molecules in system $^{50}LPS^{25}ECA_{LPS}^{25}ECA_{PG}$. In the distributions, only the Z > 0 membrane portion up to Z = 160 Å is shown after symmetrization.

As shown in **Figures 4A-B**, glycosidic torsional angle (ϕ and ψ) distributions were calculated for each sugar residue in the O159 PS (RU 2 to 4) and the ECA PS (RU 2 to 9) in two systems $^{95}\text{LPS}^5\text{ECA}_{LPS}$ and $^{50}\text{LPS}^{50}\text{ECA}_{LPS}$ to explore the conformational ensemble of LPS and ECA_{LPS}. The glycosidic torsion angles are defined as H1'-C'-Ox-Cx-(ϕ) and C1'-Ox-Cx-Hx (ψ), where x refers to the linkage position. The glycosidic torsion angles of the main states of the O159 PS and ECA PS are compiled in **Table 1** (see **Figure S6** for clustering of states). Overall, the respective glycosidic linkages exhibit similar torsional distributions and thus similar conformations of each O159 PS (RU 2 to 4) and ECA PS (RU 2 to 9) in both systems, $^{95}\text{LPS}^5\text{ECA}_{LPS}$ and $^{50}\text{LPS}^{50}\text{ECA}_{LPS}$.

The *E. coli* O159 O-antigen has as a side-chain fucosyl group in an α -(1 \rightarrow 4)-linkage to an *N*-acetylglucosamine (GlcNAc) residue, which is the branch-point of the RU (**Figure 1**). This D-GlcpNAc residue is furthermore substituted at O3 by a β -D-GlcpNAc residue of the subsequent RU, having a vicinally disubstituted trisaccharide structural element⁴⁸ of the type α -L-Fucp-(1 \rightarrow 4)[β -D-GlcpNAc-(1 \rightarrow 3)]-D-GlcpNAc. This trisaccharide structure is reminiscent of a Lewis A trisaccharide structure,⁴⁹ which has a galactose residue β -(1 \rightarrow 3)-linked instead of a D-GlcpNAc residue. For Lewis X trisaccharide structures, the substitution pattern is reversed with the fucosyl group in an α -(1 \rightarrow 3)-linkage and the D-GlcpNAc group in a β -(1 \rightarrow 4)-linkage. In a sialyl Lewis X oligosaccharide, a non-classical C-H···O hydrogen bond has been detected by NMR spectroscopy between H5 in the fucosyl group and O5 in the galactosyl residue, and MD simulations yielded an average distance of 2.6 Å for H5@Fuc-O5@Gal.⁵⁰ In a similar way, the structural element α -L-Fucp-(1 \rightarrow 3)[β -D-GlcpNAc-(1 \rightarrow 4)]-D-GlcpNAc is present in α -(1 \rightarrow 3)-fucosylated N-glycans where a H5@Fuc-O5@Gal distance of 2.6 Å or shorter was identified from NMR data, the Cambridge Structural Database and the Protein Data Bank as evidence of a C-H···O hydrogen bond.⁵¹

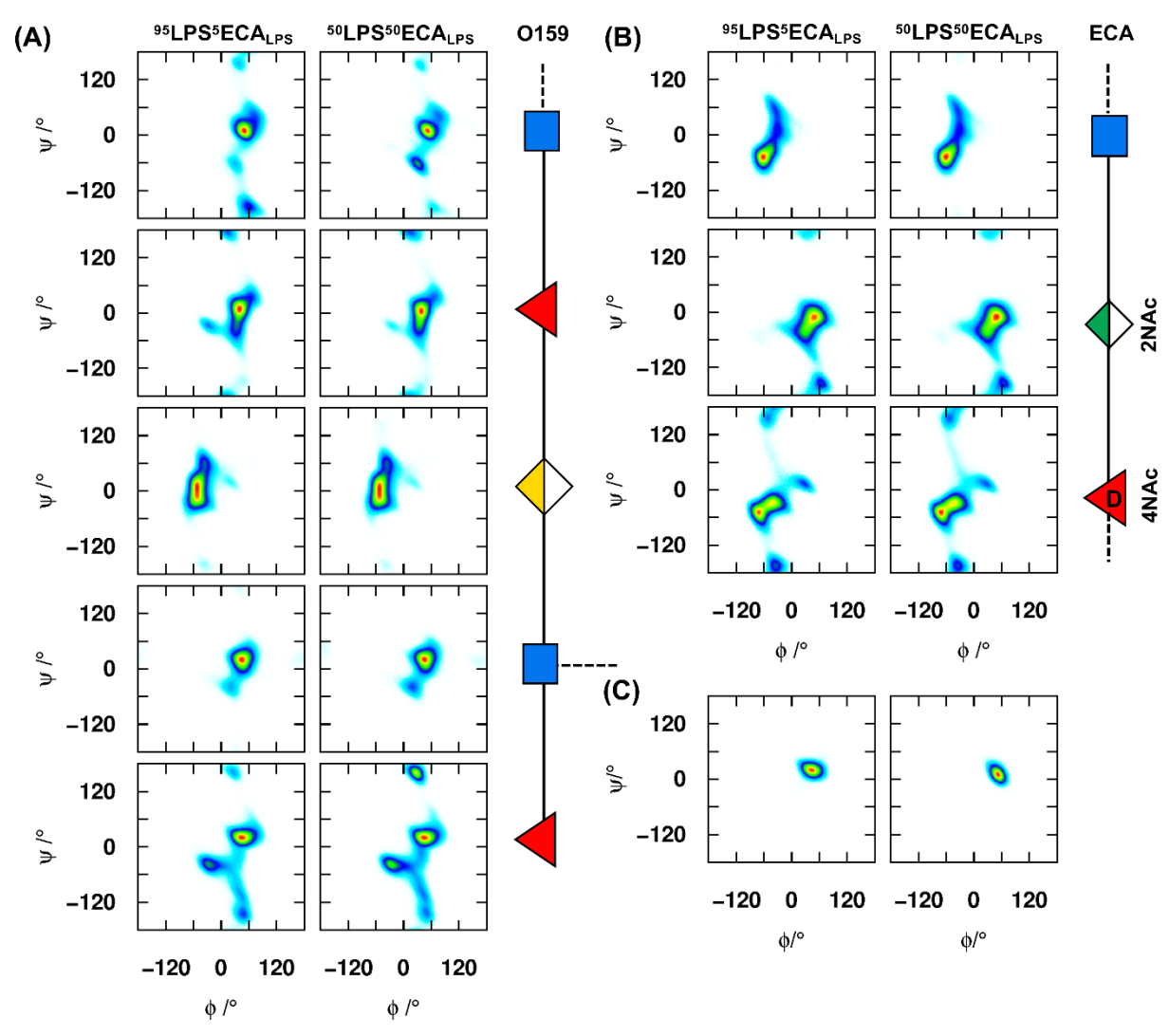


Figure 4. Two-dimensional distributions of glycosidic torsion angles (ϕ, ψ) . **(A)** O159 PS (RU 2 to 4) and **(B)** ECA PS (RU 2 to 9) in systems $^{95}\text{LPS}^5\text{ECA}_{LPS}$ and $^{50}\text{LPS}^{50}\text{ECA}_{LPS}$. **(C)** The corresponding distributions of conformations of α-L-Fucp-(1 \rightarrow 4)-D-GlcpNAc (left) and β-D-GlcpNAc-(1 \rightarrow 3)-D-GlcpNAc (right) in system ^{100}LPS for which the interatomic distance H5@Fuc (side-chain) and O5@GlcNAc (non-branched residue) is less than 2.7 Å. The density was rescaled by the maximum value: white for 0, blue for 0.1, green for 0.3, yellow for 0.7, and red for 1.

Table 1. Averaged glycosidic torsion angles (ϕ , ψ) (with standard deviations) and the population of the main state of each linkage in O159 PS and ECA PS in systems ⁹⁵LPS⁵ECA_{LPS} and ⁵⁰LPS⁵⁰ECA_{LPS}.

O159	Fuc ^a	GlcNAcb	GalA	Fuc	GlcNAc			
0159	φ (°) / ψ (°) / population (%)							
95LPS5ECA _{LPS}	49.8 ± 13.3	48.4 ± 11.2 /	-46.8 ± 12.1 /	42.5 ± 11.6 /	55.5 ± 12.2 /			
	23.4 ± 11.7 69.6	21.4 ± 13.5 / 96.6	8.0 ± 25.1 / 99.7	5.3 ± 22.4 / 93.5	17.0 ± 14.4 / 85.1			
⁵⁰ LPS ⁵⁰ ECA _{LPS}	49.3 ± 13.2 /	49.0 ± 11.2 /	-47.0 ± 12.1 /	41.2 ± 11.2 /	57.5 ± 12.3 /			
	22.2 ± 13.4 / 54.3	21.7 ± 14.1 / 93.8	7.2 ± 25.2 / 99.7	1.3 ± 21.4 / 94.3	15.9 ± 14.5 / 81.6			
ECA -	Fuc4	INAc	ManN	IAcA	GlcNAc			
	φ (°) / ψ (°) / population(%)							

	-52.9 ± 17.8 /	43.6 ± 16.2 /	-54.7 ± 11.4 /
95LPS5ECA _{LPS}	-37.1 ± 15.2 /	-18.1 ± 19.6 /	-40.6 ± 15.1 /
	85.3	93.1	81.8
	-53.8 ± 17.4 /	43.2 ± 16.4 /	-54.1 ± 11.1 /
50LPS50ECALPS	-37.5 ± 15.2 /	-17.8 ± 19.5 /	-40.5 ± 15.0 /
	86.4	92.7	83.1

^aFuc: side-chain Fuc. ^bGlcNAc: branch-point GlcNAc

To investigate which conformational state is present at the branch-points of the O159 PS, the MD trajectories were analyzed to calculate the average H5@Fuc-O5@GlcNAc distance. In all ten systems, the average H5@Fuc-O5@GlcNAc distance was always more than 3.1 Å, suggesting that a C-H···O hydrogen bond does not contribute to the stabilization of the three-dimensional structure at the branch-point regions of the O159 PS. However, as summarized in **Table S2**, there are 30% – 52% conformations showing the H5@Fuc-O5@GlcNAc distance less than 2.7 Å (i.e., the sum of their van der Waal's radii), ⁵² making significant non-classical C-H···O hydrogen bonds. These conformations at the α-L-Fucp-(1 \rightarrow 4)- and β-D-GlcpNAc-(1 \rightarrow 3)-linkages both populate an exo-anomeric $ext{syn}$ -conformation (**Figure 4C** and **Figure S7**). In addition, the ¹H NMR chemical shift of H5 of the side-chain fucosyl residue is 4.71 ppm, which is shifted significantly from 4.02 ppm of α-L-Fuc $ext{p}$ -OMe, ⁵³ influenced by the three-dimensional structural environment around the H5 hydrogen atom. Taken together, the MD simulations and the NMR chemical shift data indicate that the Lewis A type-like structural element α-L-Fuc $ext{p}$ -(1 \rightarrow 4)[β-D-Glc $ext{p}$ NAc-(1 \rightarrow 3)]-D-Glc $ext{p}$ NAc in the O159 PS is stabilized by a non-classical C-H···O hydrogen bond.

For ECA PS, the main conformational state at each glycosidic linkage corresponds to the exo-anomeric conformation ⁵⁴⁻⁵⁵ with $\phi \approx -55^{\circ}$ and $\psi \approx -40^{\circ}$ for the α -D-sugars and $\phi \approx 45^{\circ}$ and $\psi \approx -20^{\circ}$ for the β -D-sugar (**Table 1**). A comparison of our (linear ECA PS) results with a previous MD simulation⁵⁶ of a cyclic form of ECA having four RUs (ECA_{cyc-4}) shows that the glycosidic torsion angles are closely similar between the linear and cyclic forms for the two αlinked sugars ($\phi \approx -55^{\circ}$ and $\psi \approx -35^{\circ}$ in ECA_{cyc-4}), whereas the β -linked residue in ECA_{cyc-4} has $\phi/\psi \approx 60^{\circ}/0^{\circ}$ or $\phi/\psi \approx 85^{\circ}/60^{\circ}$, thus deviating substantially from the linear form of ECA PS. In a crystal structure of ECA_{cyc-4} having two forms, a rhomboid and a square form,⁵⁷ it is the α -D-Fuc4NAc residues that show a larger spread of the glycosidic torsion angles where ϕ and ψ are linearly correlated, reminiscent of the syn-conformations in the central region of the ϕ/ψ distribution maps of the ECA PS (**Figure 4B**). The crystal structure shows $\phi \approx 45^{\circ}$ for the β-D-ManpNAcA residues, i.e, the exo-anomeric conformation, but $\psi \approx 15^\circ$ deviating significantly from the linear ECA PS. Thus, from the previous MD simulation of ECA_{cvc-4} in solution and from the crystal structures of the cyclic form, most glycosidic torsions populate a similar conformational space to those of the linear ECA PS, except for ψ of the β -D-ManpNAcA residue, which is shifted to the region with a positive value of its torsion angle.

Properties of LPS and ECA Bilayers

The hydrophobic thickness is an important measure that affects the structures and activities of membrane proteins and peptides. The calculated average hydrophobic thickness of each system is shown in **Figure 5**. Carbons in the red circles in **Figure S1** were used for the thickness calculation. It is evident that there is a dramatic decrease in the hydrophobic thickness when population of ECA_{PG} is increased. For the pure O159 LPS system (100 LPS), the average thickness is 20.1 ± 0.2 Å. The four 95% LPS systems show similar thicknesses: 19.7 ± 0.2 Å (95 LPS 5 ECA_{LPS}), 19.8 ± 0.2 Å (95 LPS 5 ECA_{PVPG}), 20.1 ± 0.4 Å (95 LPS 5 ECA_{DPPG}), and 20.0 ± 0.1 Å (95 LPS 5 ECA_{PSPG}). The average hydrophobic thickness is also comparable for 75 LPS 25 ECA_{LPS} (19.8 ± 0.1 Å) and 50 LPS 50 ECA_{LPS} (19.6 ± 0.1 Å). With 25% ECA_{PG}, the average thickness decreases to 18.9 ± 0.2 Å (75 LPS 25 ECA_{PG}) and 18.6 ± 0.1 Å (50 LPS 25 ECA_{LPS} 25 ECA_{PG}).

When 50% ECA_{PG} is included, the average thickness becomes only 16.5 \pm 0.2 Å. The decreased trend of the hydrophobic thickness along with the increased population of ECA_{PG} indicates that ECA_{PG} affects the structural and dynamic properties of the lipid portion of each LPS and ECA in the membrane systems (**Figure S3**).

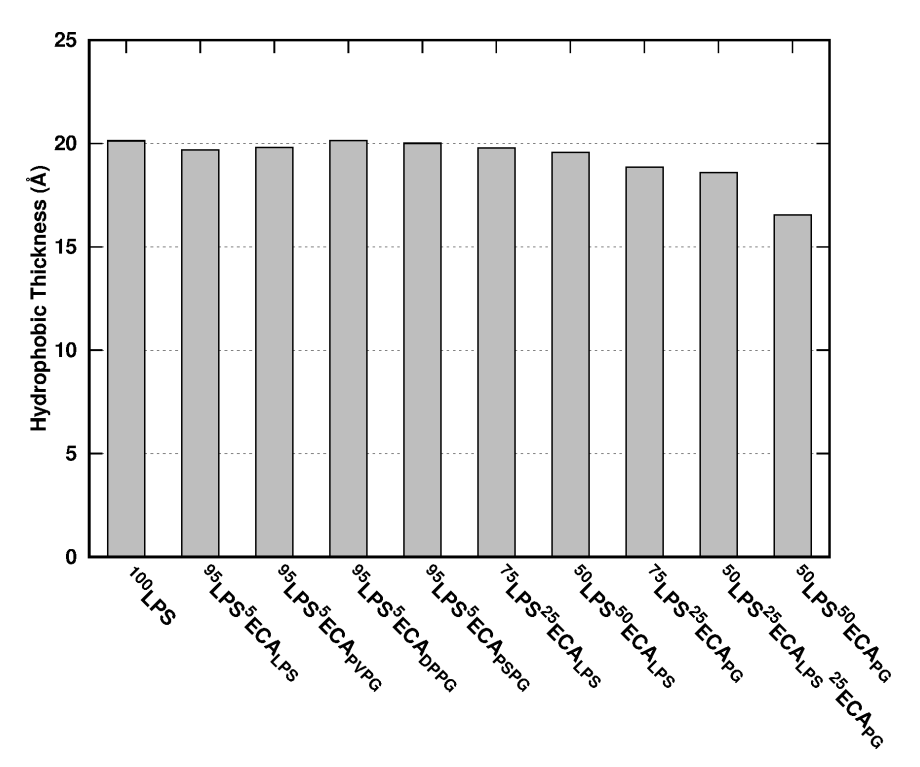


Figure 5. Averaged hydrophobic thickness.

The order parameters (S_{CD}) of lipid acyl chains are used to provide information regarding the overall order of the membrane: $S_{CD} = |\langle 3 \times \cos^2(\theta_{CH}) - 1 \rangle/2|$, where θ_{CH} is the angle between a C-H bond vector and the Z axis, and the bracket represents the time and ensemble average. Figure 6 shows the calculated order parameters of acyl chain 6 for lipid A and acyl chain 2 for PVPG/DPPG/PSPG. For the lipid A of LPS, the order parameters of each ¹⁰⁰LPS, ⁹⁵LPS⁵ECA_{LPS}, ⁹⁵LPS⁵ECA_{PVPG}, ⁹⁵LPS⁵ECA_{DPPG}, ⁹⁵LPS⁵ECA_{PSPG}, ⁷⁵LPS²⁵ECA_{LPS}, and ⁵⁰LPS⁵⁰ECA_{LPS} overlap well, indicating the similar structural and dynamic mode for the LPS lipid A acyl chain sampled during simulations. Two 25% ECA_{PG} systems, ⁷⁵LPS²⁵ECA_{PG} and ⁵⁰LPS²⁵ECA_{LPS}²⁵ECA_{PG}, exhibit a similar trend showing more disordered lipid A compared to other systems except 50LPS50ECAPG in which the lipid A is the most disordered, indicated by the lowest S_{CD} . The decreased trend of the S_{CD} along with the increasing population of ECA_{PG} is also observed for lipid A acyl chain 6 of ECA_{LPS}, and acyl chain 2 of ECA_{PVPG}/ECA_{DPPG}/ECA_{PSPG} (Figure 6). The result is consistent with the analyses of pairwise RMSD of lipid tails (Figure S3) and the hydrophobic thickness (Figure 5), indicating that incorporation of ECA_{PG} makes the acyl chains of each glycolipid more flexible and disordered.

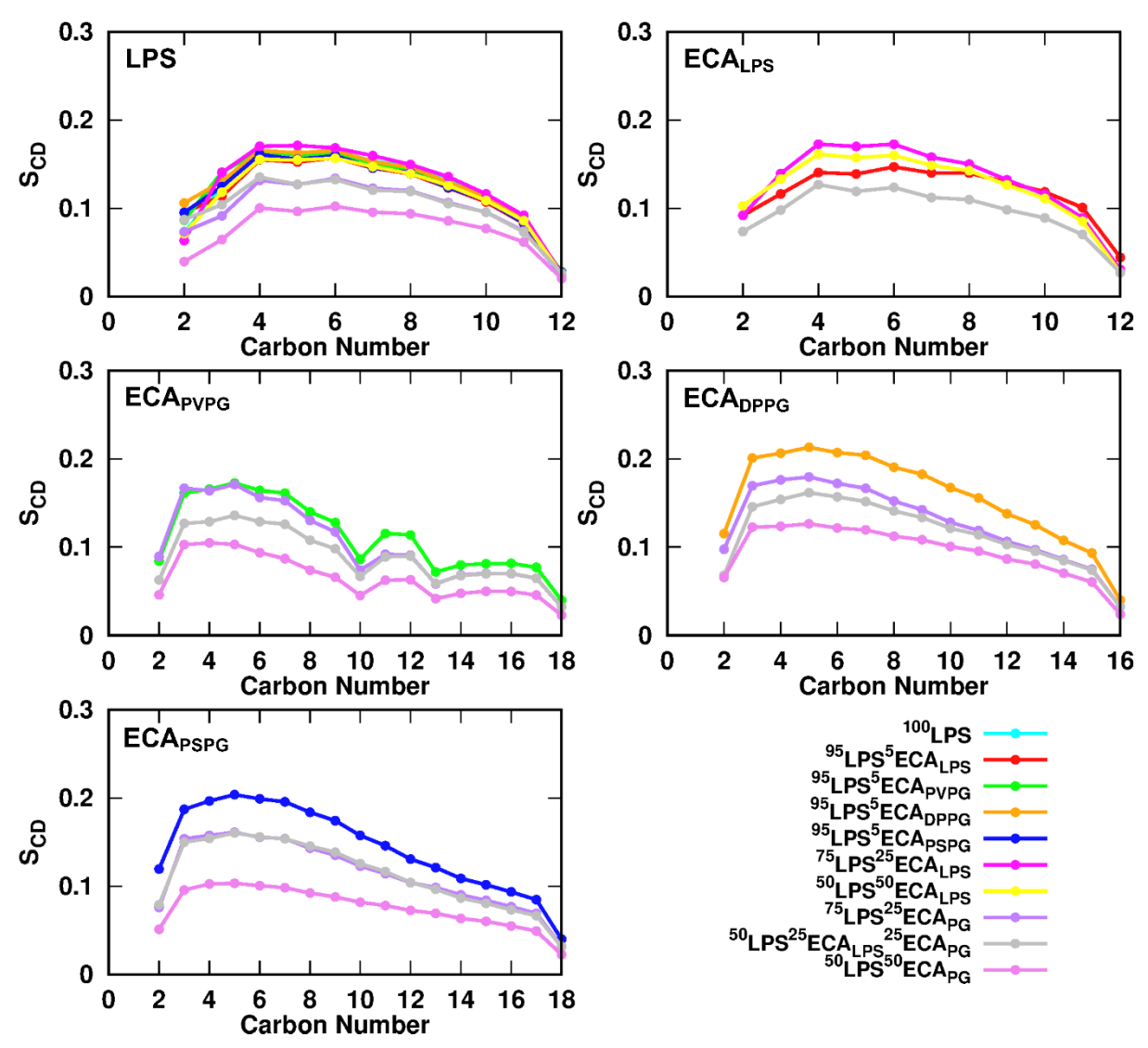


Figure 6. Calculated chain order parameters of acyl chain 6 of lipid A and acyl chain 2 of PVPG/DPPG/PSPG (see **Figure S1** for the chain number).

The area per lipid (APL) provides important information about lipid packing in a bilayer resulting from attractions among head groups and repulsions among non-polar hydrocarbon tails. However, when the membrane composition is mixed, interactions between neighboring lipids lead to the change in the average APL. In this work, the APL was calculated using the Voronoi tessellation method and averaged over the lipids. Carbons in the red circles of lipid A and those in the blue circles of PVPG/DPPG/PSPG in Figure S1 were used in the Voronoi tessellation calculation^{30, 58} for LPS, ECA_{LPS}, and ECA_{PG}. **Table 2** summarizes the APL of each LPS and ECA. The APL is estimated to be 190 Å² for *E. coli* LPS5 (5 RUs of O6-antigen) in the previous work.⁵ In the work of Kucerka et al., the APL of POPG at 30°C was determined to be 66.1 Å² by using small angle neutron and X-ray scattering tools.⁵⁹ In system ¹⁰⁰LPS, the APL is 192 Å², which is comparable to the previous work. When 5% ECA_{PG} is mixed, the APL of LPS increases somewhat to 193~197 Å². When 25% and 50% ECA_{LPS} are incorporated, the APL of LPS increases to 196 Å² and 199 Å², respectively. In ⁷⁵LPS²⁵ECA_{PG} and ⁵⁰LPS²⁵ECA_{LPS}²⁵ECA_{PG} systems, the APL of LPS increases by ~16 Å² compared to that of ¹⁰⁰LPS. In ⁵⁰LPS⁵⁰ECA_{PG}, the APL of LPS increases to 236 Å², indicating that the acyl chains of lipid A are more disordered and flexible compared to those of ¹⁰⁰LPS. Correspondingly, the APLs of ECA_{LPS} and ECA_{PG} also increase along with the increasing population of ECA_{PG}, and

in ⁵⁰LPS⁵⁰ECA_{PG}, the APL of each glycolipid becomes largest among the current systems (**Table 2**).

Table 2. Calculated area per lipid with standard errors for each LPS and ECA in the respective system.

A							
Simulated systems	Area per lipid (Ų)						
	LPS	ECA LPS	ECA _{PVPG}	ECADPPG	ECA _{PSPG}		
¹⁰⁰ LPS	192.0 ± 0.8						
95LPS5ECA _{LPS}	196.3 ± 1.6	196.6 ± 7.9					
95LPS5ECA _{PVPG}	196.9 ± 1.2		77.7 ± 6.2				
95LPS5ECADPPG	192.9 ± 3.5			65.4 ± 4.6			
95LPS5ECA _{PSPG}	194.2 ± 1.3				72.4 ± 5.9		
75LPS25ECALPS	196.0 ± 1.4	194.4 ± 3.3					
50LPS50ECALPS	199.0 ± 2.3	196.6 ± 1.9					
75LPS ²⁵ ECA _{PG}	208.9 ± 1.9		78.0 ± 3.6	77.0 ± 2.4	77.1 ± 5.9		
⁵⁰ LPS ²⁵ ECA _{LPS} ²⁵ ECA _{PG}	209.9 ± 3.1	216.0 ± 6.3	83.0 ± 4.9	78.5 ± 3.6	80.4 ± 5.8		
⁵⁰ LPS ⁵⁰ ECA _{PG}	235.9 ± 4.1		96.9 ± 5.1	89.3 ± 2.6	96.9 ± 4.4		

For ⁷⁵LPS²⁵ECA_{LPS} and ⁵⁰LPS⁵⁰ECA_{LPS}, the possible reason for the increased APL of LPS compared to that in ¹⁰⁰LPS could be the stronger electrostatic repulsive interaction among ECA_{LPS} RUs. In LPS and ECA_{LPS}, the lipid A and core region have the same charge (-4e for lipid A and -5e for the core). However, the total charge of ECA PS repeating units is -10e (-1e for ManNAcA in each RU, 10 RUs in total), larger than that of O159 PS repeating units (-1e for GalA in each RU, 5 RUs in total). The larger repulsive interaction tends to make more space for LPS molecules, so the acyl chains have more flexible and dynamic conformation sampled. As mentioned above, in ¹⁰⁰LPS, ⁹⁵LPS⁵ECA_{PVPG/DPPG/PSPG}, ⁷⁵LPS²⁵ECA_{PG}, ⁵⁰LPS²⁵ECA_{PG}, and ⁵⁰LPS⁵⁰ECA_{PG}, the APL of LPS increases gradually from 192, 196, 209, to 236 Å². In our previous work, ⁶⁰ with more DPPC mixed with LPS molecules, DPPC lipids interspersed in the gaps between LPS molecules, resulting in the decrease of the APL of LPS and thus tightly packed membranes. In the current work, instead of having individual DPPC lipids, ECA RUs are linked to PVPG/DPPG/PSPG, forming the ECA_{PG} that is not possible to intersperse in the gaps between LPS molecules due to the steric interactions among O159 PS and ECA PS RUs. So, the possible reason for the increase of APL when more ECA_{PG} mixed with LPS could be the same electrostatic repulsive interaction among ECA RUs and core and O159 PS regions, but with only two acyl chains in the ECA_{PG}, more space becomes available for the acyl chains of LPS and ECA_{PG}, resulting in loosely packed membranes.

Conclusions

ECA is a surface antigen shared by all members of the *Enterobacteriaceae* family. It is important for cell envelope integrity, flagellum expression, and resistance of enteric bacteria to acetic acid and bile salts. ECA occurs in three forms. The major form of ECA (ECA_{PG}), which is found in all members of the *Enterobacteriaceae*, consists of polysaccharides that are covalently linked to diacylglycerol through phosphodiester linkage. In ECA_{LPS}, the ECA polysaccharide moiety is linked to the core region of the LPS. ECA_{CYC} is a cyclic, water soluble oligosaccharide that contains a different number of trisaccharide repeating units often acetylated at O-6 of the GlcNAc residue.¹⁹ The two minor forms of ECA (ECA_{LPS} and ECA_{CYC}) have been identified in certain Gram-negative bacteria. The biological significance of ECA

remains elusive, but it is reported that ECA is needed for the expression of the full pathogenic capacity of the bacteria.

In the previous modeling and simulation of bacterial OMs, the outer leaflet was made of LPS, but devoid of ECA molecules. In this work, ECA as a glycolipid form, ECA_{PG}, and in an LPS form, ECA_{LPS}, are modeled and incorporated into symmetric E. coli O159 LPS bilayers in different ratios, and simulations are performed to investigate the LPS and ECA conformations and the bilayer properties. Pairwise RMSD shows that dynamic and flexible conformations are sampled for each LPS and ECA with broad RMSD distributions in each system. The major conformational states of O159 LPS and ECA polysaccharides have the exo-anomeric syn-conformations at their glycosidic linkages. The side-chain fucosyl residue of O159 O-antigen is proposed to be stabilized by a non-classical C-H···O hydrogen bond between H5 of fucose and O5 of a main-chain GlcNAc residue, which can be revealed by specific NMR experiments to be carried out due course. The decreased hydrophobic thickness and order parameters of lipid A and PVPG/DPPG/PSPG along with the increased population of ECA_{PG} indicate that ECA_{PG} affects the structural and dynamic properties of each glycolipid in the membrane system, and incorporation of ECA_{PG} makes the acyl chains of each glycolipid more flexible and disordered. These results are consistent with the calculated APL results for each glycolipid, indicating that the APLs of LPS and ECA increase along with the increase of the population of ECA_{PG}. The calculated APLs for each glycolipid in each system with different ratios of ECA can provide a better estimate for building more realistic OMs containing ECA for future studies.

Acknowledgement

This work was supported in part by grants from the NSF MCB-1727508, NSF MCB-1810695, XSEDE MCB070009, Friedrich Wilhelm Bessel Research Award from the Humboldt foundation (to WI), and the Swedish Research Council 2017-03703 (GW).

Supporting Information

Molecular dynamics simulation system information; averaged glycosidic torsion angles (ϕ,ψ) of α-L-Fucp-(1→4)-D-GlcpNAc and β-D-GlcpNAc-(1→3)-D-GlcpNAc in O159-PS (RU 2 to 4) for which the interatomic distance H5@Fuc (side-chain) and O5@GlcNAc (non-branched residue) is less than 2.7 Å.; chemical structures of *E. coli* lipid A, PVPG, DPPG, and PSPG; time-series of X or Y system length; pairwise RMSD distributions for residue 1 (i.e., lipid A or phosphatidylglycerol lipids) and all sugars (i.e., except for residue 1) of each LPS and ECA; distributions of ions and charged moieties of LPS (Ca²+, PO₄²-, and COO⁻) along the Z-axis in system 50 LPS 25 ECA_{LPS} 25 ECA_{PG}; glycosidic torsion angle distributions for each linkage of O159-PS and ECA-PS in systems 95 LPS 50 ECA_{LPS} 50 ECA_{LPS}; two-dimensional distributions of glycosidic torsion angles (ϕ , ψ) of conformations of α-L-Fucp-(1→4)-D-GlcpNAc and β-D-GlcpNAc-(1→3)-D-GlcpNAc in O159-PS (RU 2 to 4) for which the interatomic distance H5@Fuc (side-chain) and O5@GlcNAc (non-branched residue) is less than 2.7 Å.

References

- 1. Kamio, Y.; Nikaido, H., Outer Membrane of Salmonella Typhimurium Accessibility of Phospholipid Head Groups to Phospholipase-C and Cyanogen-Bromide Activated Dextrain in External Medium. *Biochemistry* **1976**, *15*, 2561-2570.
- 2. Smit, J.; Kamio, Y.; Nikaido, H., Outer Membrane of Salmonella Typhimurium Chemical Analysis and Freeze Fracture Studies with Lipopolysaccharide Mutants. *J. Bacteriol.* **1975**, *124*, 942-958.
- 3. Kuhn, H. M.; Meierdieter, U.; Mayer, H., Eca, the Enterobacterial Common Antigen. *Fems Microbiol. Rev.* **1988**, *54*, 195-222.
- 4. Whitfield, C., Biosynthesis and Assembly of Capsular Polysaccharides in Escherichia Coli. *Annu. Rev. Biochem.* **2006,** *75*, 39-68.
- 5. Wu, E. L.; Engstrom, O.; Jo, S.; Stuhlsatz, D.; Yeom, M. S.; Klauda, J. B.; Widmalm, G.; Im, W., Molecular Dynamics and Nmr Spectroscopy Studies of E. Coli Lipopolysaccharide Structure and Dynamics. *Biophys. J.* **2013**, *105*, 1444-1455.
- 6. Ma, H. L.; Irudayanathan, F. J.; Jiang, W. J.; Nangia, S., Simulating Gram-Negative Bacterial Outer Membrane: A Coarse Grain Model. *J. Phys. Chem. B* **2015**, *119*, 14668-14682.
- 7. Blasco, P.; Patel, D. S.; Engstrom, O.; Im, W.; Widmalm, G., Conformational Dynamics of the Lipopolysaccharide from Escherichia Coli O91 Revealed by Nuclear Magnetic Resonance Spectroscopy and Molecular Simulations. *Biochemistry* **2017**, *56*, 3826-3839.
- 8. Li, A.; Schertzer, J. W.; Yong, X., Molecular Dynamics Modeling of Pseudomonas Aeruginosa Outer Membranes. *Phys. Chem. Chem. Phys.* **2018**, *20*, 23635-23648.
- 9. Piggot, T. J.; Holdbrook, D. A.; Khalid, S., Electroporation of the E. Coli and S. Aureus Membranes: Molecular Dynamics Simulations of Complex Bacterial Membranes. *J. Phys. Chem. B* **2011**, *115*, 13381-13388.
- 10. Lee, J.; Pothula, K. R.; Kleinekathofer, U.; Im, W., Simulation Study of Occk5 Functional Properties in Pseudomonas Aeruginosa Outer Membranes. *J. Phys. Chem. B* **2018**, *122*, 8185-8192.
- 11. Wu, E. L.; Fleming, P. J.; Yeom, M. S.; Widmalm, G.; Klauda, J. B.; Fleming, K. G.; Im, W., E. Coli Outer Membrane and Interactions with Ompla. *Biophys. J.* **2014**, *106*, 2493-2502.
- 12. Shearer, J.; Jefferies, D.; Khalid, S., Outer Membrane Proteins Ompa, Fhua, Ompf, Esta, Btub, and Ompx Have Unique Lipopolysaccharide Fingerprints. *J. Chem. Theory Comput.* **2019**, *15*, 2608-2619.
- 13. Im, W.; Khalid, S., Molecular Simulations of Gram-Negative Bacterial Membranes Come of Age. *Annu. Rev. Phys. Chem.* **2020**, *71*, 8.1-8.18.
- 14. Patel, D. S.; Qi, Y. F.; Im, W., Modeling and Simulation of Bacterial Outer Membranes and Interactions with Membrane Proteins. *Curr. Res. Struct. Biol.* **2017**, *43*, 131-140.
- 15. Hwang, H.; Paracini, N.; Parks, J. M.; Lakey, J. H.; Gumbart, J. C., Distribution of Mechanical Stress in the Escherichia Coli Cell Envelope. *BBA-Biomembranes* **2018**, *1860*, 2566-2575.
- 16. Patel, D. S.; Re, S.; Wu, E. L.; Qi, Y. F.; Klebba, P. E.; Widmalm, G.; Yeom, M. S.; Sugita, Y.; Im, W., Dynamics and Interactions of Ompf and Lps: Influence on Pore Accessibility and Ion Permeability. *Biophys. J.* **2016**, *110*, 930-938.
- 17. Gozdziewicz, T. K.; Lugowski, C.; Lukasiewicz, J., First Evidence for a Covalent Linkage between Enterobacterial Common Antigen and Lipopolysaccharide in Shigella Sonnei Phase li Ecalps. *J. Biol. Chem.* **2014**, 289, 2745-2754.
- 18. Gozdziewicz, T. K.; Lugowski, C.; Lukasiewicz, J., First Evidence for a Covalent Linkage between Enterobacterial Common Antigen and Lipopolysaccharide in Shigella Sonnei Phase li Eca(Lps). *J. Biol. Chem.* **2018**, 293, 11652-11653.
- 19. Dell, A.; Oates, J.; Lugowski, C.; Romanowska, E.; Kenne, L.; Lindberg, B., The Enterobacterial Common-Antigen, a Cyclic Polysaccharide. *Carbohyd. Res.* **1984**, *133*, 95-104.
- 20. Lugowski, C.; Romanowska, E.; Kenne, L.; Lindberg, B., Identification of a Trisaccharide Repeating-Unit in the Enterobacterial Common-Antigen. *Carbohyd. Res.* **1983**, *118*, 173-181.

- 21. Fregolino, E.; Ivanova, R.; Lanzetta, R.; Molinaro, A.; Parrilli, M.; Paunova-Krasteva, T.; Stoitsova, S. R.; De Castro, C., Occurrence and Structure of Cyclic Enterobacterial Common Antigen in Escherichia Coli O157:H. *Carbohyd. Res.* **2012**, 363, 29-32.
- 22. Andersson, A.; Ahl, A.; Eklund, R.; Widmalm, G.; Maler, L., Dynamics in the Cyclic Enterobacterial Common Antigen as Studied by C-13 Nmr Relaxation. *J. Biomol. NMR* **2005**, 31, 311-320.
- 23. Kuhn, H. M.; Basu, S.; Mayer, H., Comparison of Enterobacterial Common Antigen from Different Species by Serological Techniques. *J. Biochem.* **1987**, *162*, 69-74.
- 24. Rick, P. D.; Hubbard, G. L.; Kitaoka, M.; Nagaki, H.; Kinoshita, T.; Dowd, S.; Simplaceanu, V.; Ho, C., Characterization of the Lipid-Carrier Involved in the Synthesis of Enterobacterial Common Antigen (Eca) and Identification of a Novel Phosphoglyceride in a Mutant of Salmonella Typhimurium Defective in Eca Synthesis. *Glycobiology* **1998**, *8*, 557-567.
- 25. de Vlugt, J. E.; Xiao, P.; Munro, R.; Charchoglyan, A.; Brewer, D.; Al-Abdul-Wahid, M. S.; Brown, L. S.; Ladizhansky, V., Identifying Lipids Tightly Bound to an Integral Membrane Protein. *BBA-Biomembranes* **2020**, in press, https://doi.org/10.1016/j.bbamem.2020.183345.
- 26. Duda, K. A.; Duda, K. T.; Beczala, A.; Kasperkiewicz, K.; Radziejewska-Lebrecht, J.; Skurnik, M., Eca-Immunogenicity of Proteus Mirabilis Strains. *Arch. Immunol. Ther. Ex.* **2009**, *57*, 147-151.
- 27. Linnerborg, M.; Weintraub, A.; Widmalm, G., Structural Studies Utilizing C-13-Enrichment of the O-Antigen Polysaccharide from the Enterotoxigenic Escherichia Coli O159 Cross-Reacting with Shigella Dysenteriae Type 4. *J. Biochem.* **1999**, *266*, 246-251.
- 28. Patel, D. S.; Blasco, P.; Widmalm, G.; Im, W., Escherichia Coli O176 Lps Structure and Dynamics: A Nmr Spectroscopy and Md Simulation Study. *Curr. Res. Struct. Biol.* **2020**, 2, 79-88.
- 29. Jo, S.; Kim, T.; Im, W., Automated Builder and Database of Protein/Membrane Complexes for Molecular Dynamics Simulations. *Plos One* **2007**, *2*, e880.
- 30. Jo, S.; Lim, J. B.; Klauda, J. B.; Im, W., Charmm-Gui Membrane Builder for Mixed Bilayers and Its Application to Yeast Membranes. *Biophys. J.* **2009**, *97*, 50-58.
- 31. Wu, E. L.; Cheng, X.; Jo, S.; Rui, H.; Song, K. C.; Davila-Contreras, E. M.; Qi, Y. F.; Lee, J. M.; Monje-Galvan, V.; Venable, R. M.; Klauda, J. B.; Im, W., Charmm-Gui Membrane Builder toward Realistic Biological Membrane Simulations. *J. Comput. Chem.* **2014**, *35*, 1997-2004.
- 32. Lee, J.; Cheng, X.; Swails, J. M.; Yeom, M. S.; Eastman, P. K.; Lemkul, J. A.; Wei, S.; Buckner, J.; Jeong, J. C.; Qi, Y. F.; Jo, S.; Pande, V. S.; Case, D. A.; Brooks, C. L.; MacKerell, A. D.; Klauda, J. B.; Im, W., Charmm-Gui Input Generator for Namd, Gromacs, Amber, Openmm, and Charmm/Openmm Simulations Using the Charmm36 Additive Force Field. *J. Chem. Theory Comput.* **2016**, *12*, 405-413.
- 33. Lee, J.; Patel, D. S.; Stahle, J.; Park, S. J.; Kern, N. R.; Kim, S.; Lee, J.; Cheng, X.; Valvano, M. A.; Holst, O.; Knirel, Y. A.; Qi, Y. F.; Jo, S.; Klauda, J. B.; Widmalm, G.; Im, W., Charmm-Gui Membrane Builder for Complex Biological Membrane Simulations with Glycolipids and Lipoglycans. *J. Chem. Theory Comput.* **2019**, *15*, 775-786.
- 34. Jo, S.; Kim, T.; Iyer, V. G.; Im, W., Software News and Updates Charnim-Gui: A Web-Based Grraphical User Interface for Charmm. *J. Comput. Chem.* **2008**, 29, 1859-1865.
- 35. Kim, S.; Patel, D. S.; Park, S.; Slusky, J.; Klauda, J. B.; Widmalm, G.; Im, W., Bilayer Properties of Lipid a from Various Gram-Negative Bacteria. *Biophys. J.* **2016**, *111*, 1750-1760.
- 36. Jo, S.; Wu, E. L.; Stuhlsatz, D.; Klauda, J. B.; MacKerell, A. D.; Widmalm, G.; Im, W., Lipopolysaccharide Membrane Building and Simulation. In *Glycoinformatics*, Lütteke, T.; Frank, M., Eds. Springer New York: New York, NY, 2015.
- 37. Klauda, J. B.; Venable, R. M.; Freites, J. A.; O'Connor, J. W.; Tobias, D. J.; Mondragon-Ramirez, C.; Vorobyov, I.; MacKerell, A. D.; Pastor, R. W., Update of the Charmm All-Atom Additive Force Field for Lipids: Validation on Six Lipid Types. *J. Phys. Chem. B* **2010**, *114*, 7830-7843.

- 38. Guvench, O.; Greene, S. N.; Kamath, G.; Brady, J. W.; Venable, R. M.; Pastor, R. W.; Mackerell, A. D., Additive Empirical Force Field for Hexopyranose Monosaccharides. *J. Comput. Chem.* **2008**, *29*, 2543-2564.
- 39. Guvench, O.; Hatcher, E.; Venable, R. M.; Pastor, R. W.; MacKerell, A. D., Charmm Additive All-Atom Force Field for Glycosidic Linkages between Hexopyranoses. *J. Chem. Theory Comput.* **2009**, *5*, 2353-2370.
- 40. Hatcher, E.; Guvench, O.; MacKerell, A. D., Charmm Additive All-Atom Force Field for Aldopentofuranoses, Methyl-Aldopentofuranosides, and Fructofuranose. *J. Phys. Chem. B* **2009**, *113*, 12466-12476.
- 41. Guvench, O.; Mallajosyula, S. S.; Raman, E. P.; Hatcher, E.; Vanommeslaeghe, K.; Foster, T. J.; Jamison, F. W.; MacKerell, A. D., Charmm Additive All-Atom Force Field for Carbohydrate Derivatives and Its Utility in Polysaccharide and Carbohydrate-Protein Modeling. *J. Chem. Theory Comput.* **2011,** 7, 3162-3180.
- 42. Ryckaert, J. P.; Ciccotti, G.; Berendsen, H. J. C., Numerical-Integration of Cartesian Equations of Motion of a System with Constraints-Molecular-Dynamics of N-Alkanes. *J. Comput. Phys.* **1977**, 23, 327-341.
- 43. Steinbach, P. J.; Brooks, B. R., New Spherical-Cutoff Methods for Long-Range Forces in Macromolecular Simulation. *J. Comput. Chem.* **1994**, *15*, 667-683.
- 44. Essmann, U.; Perera, L.; Berkowitz, M. L.; Darden, T.; Lee, H.; Pedersen, L. G., A Smooth Particle Mesh Ewald Method. *J. Chem. Phys.* **1995**, *103*, 8577-8593.
- 45. Chow, K. H.; Ferguson, D. M., Isothermal Isobaric Molecular-Dynamics Simulations with Monte-Carlo Volume Sampling. *Comput. Phys. Commun.* **1995**, *91*, 283-289.
- 46. Aqvist, J.; Wennerstrom, P.; Nervall, M.; Bjelic, S.; Brandsdal, B. O., Molecular Dynamics Simulations of Water and Biomolecules with a Monte Carlo Constant Pressure Algorithm. *Chem. Phys. Lett.* **2004**, *384*, 288-294.
- 47. Eastman, P.; Friedrichs, M. S.; Chodera, J. D.; Radmer, R. J.; Bruns, C. M.; Ku, J. P.; Beauchamp, K. A.; Lane, T. J.; Wang, L. P.; Shukla, D.; Tye, T.; Houston, M.; Stich, T.; Klein, C.; Shirts, M. R.; Pande, V. S., Openmm 4: A Reusable, Extensible, Hardware Independent Library for High Performance Molecular Simulation. *J. Chem. Theory Comput.* **2013**, *9*, 461-469.
- 48. Soderman, P.; Jansson, P. E.; Widmalm, G., Synthesis, Nmr Spectroscopy and Conformational Studies of the Four Anomeric Methyl Glycosides of the Trisaccharide D-Glcp-(1->3) D-Glcp-(1->4) -Alpha-D-Glcp. *J. Chem. Soc., Perkin Trans.* 2 **1998**, 639-648.
- 49. Sawen, E.; Hinterholzinger, F.; Landersjo, C.; Widmalm, G., Conformational Flexibility of the Pentasaccharide Lnf-2 Deduced from Nmr Spectroscopy and Molecular Dynamics Simulations. *Org. Biomol. Chem.* **2012**, *10*, 4577-4585.
- 50. Battistel, M. D.; Azurmendi, H. F.; Frank, M.; Freedberg, D. I., Uncovering Nonconventional and Conventional Hydrogen Bonds in Oligosaccharides through Nmr Experiments and Molecular Modeling: Application to Sialyl Lewis-X. *J. Am. Chem. Soc.* **2015**, *137*, 13444-13447.
- 51. Aeschbacher, T.; Zierke, M.; Smiesko, M.; Collot, M.; Mallet, J. M.; Ernst, B.; Allain, F. H. T.; Schubert, M., A Secondary Structural Element in a Wide Range of Fucosylated Glycoepitopes. *Chem-Eur. J.* **2017**, 23, 11598-11610.
- 52. Alvarez, S., A Cartography of the Van Der Waals Territories. *Dalton Trans.* **2013**, *42*, 8617-8636.
- 53. Jansson, P. E.; Kenne, L.; Widmalm, G., Computer-Assisted Structural-Analysis of Oligosaccharides Using Casper. *Anal. Biochem.* **1991**, *199*, 11-17.
- 54. Lemieux, R. U.; Koto, S., The Conformational Properties of Glycosidic Linkages. *Tetrahedron* **1974**, *30*, 1933-1944.
- 55. Eklund, R.; Widmalm, G., Molecular Dynamics Simulations of an Oligosaccharide Using a Force Field Modified for Carbohydrates. *Carbohyd. Res.* **2003**, 338, 393-398.
- 56. Staaf, M.; Hoog, C.; Stevensson, B.; Maliniak, A.; Widmalm, G., Conformational Investigation of a Cyclic Enterobacterial Common Antigen Employing Nmr Spectroscopy and Molecular Dynamics Simulations. *Biochemistry* **2001**, *40*, 3623-3628.

- 57. Farnback, M.; Eriksson, L.; Senchenkova, S.; Zych, K.; Knirel, Y. A.; Sidorczyk, Z.; Widmalm, G., Crystal Structure of a Cyclic Enterobacterial Common Antigen. *Angew. Chem. Int. Edit.* **2003**, *42*, 2543-2546.
- 58. Patel, D. S.; Park, S.; Wu, E. L.; Yeom, M. S.; Widmalm, G.; Klauda, J. B.; Im, W., Influence of Ganglioside Gm1 Concentration on Lipid Clustering and Membrane Properties and Curvature. *Biophys. J.* **2016**, *111*, 1987-1999.
- 59. Pan, J. J.; Heberle, F. A.; Tristram-Nagle, S.; Szymanski, M.; Koepfinger, M.; Katsaras, J.; Kucerka, N., Molecular Structures of Fluid Phase Phosphatidylglycerol Bilayers as Determined by Small Angle Neutron and X-Ray Scattering. *BBA-Biomembranes* **2012**, *1818*, 2135-2148.
- 60. Hughes, A. V.; Patel, D. S.; Widmalm, G.; Klauda, J. B.; Clifton, L. A.; Im, W., Physical Properties of Bacterial Outer Membrane Models: Neutron Reflectometry & Molecular Simulation. *Biophys. J.* **2019**, *116*, 1095-1104.

